48th AIAA Aerospace Sciences Meeting Including the New Horizons Forum and Aerospace Exposition
4 - 7 January 2010, Orlando, Florida

AIAA 2010-86

Hybrid Control of a Turret Wake, Part I: Aerodynamic Effects

Bojan Vukasinovic*, Ari Glezer†,
Woodruff School of Mechanical Engineering,
Georgia Institute of Technology, Atlanta, GA 30332-0405

Stanislav Gordeyev‡, Eric Jumper§,
Department of Aerospace and Mechanical Engineering,
University of Notre Dame, Notre Dame, IN 46556

Valdis Kibens**
The Boeing Company, MC S306-430,
P.O. Box 516, Saint Louis, MO 63166

Effects of active and hybrid flow control on the aerodynamic characteristics of flow over a 0.254 m diameter conformal optical aperture embedded in the hemispherical cap of a cylinder turret model (D = 0.61 m) are investigated at M = 0.3 – 0.5 and Re_D = 4.4–7.4·10^6. Resulting mean flows are characterized by surface static pressure distributions and oil-flow visualizations, while the separated flow dynamics is assessed by hot-film measurements. Active flow control is effected by arrays of piezoelectrically-driven synthetic jet modules distributed in multiple arrays upstream from the aperture. Active flow control is further assisted by global flow alterations induced by a passive forward partition plate, and, when combined, constitute hybrid flow control. It is shown that the hybrid flow control combines the positive effects of its component control elements to yield superior results in any cumulative aerodynamic aspect of the separated flow. This cumulative effect of the actuation is manifested by concomitant delay of flow separation and active, dissipative suppression of turbulent motions downstream of separation. It is also demonstrated by means of direct 2D wavefront measurements that the overall aerodynamic improvements correlate with substantial suppression of optical aberrations through the separated flow. Furthermore, estimated Strehl ratios for the laser beam indicate that nearly-invariant Strehl ratio is established within the range of tested aperture elevation angles, yielding improvement of about 50% for the highest elevation angle.

Nomenclature

A_j	=	exit area of the actuator orifice
A_o	=	frontal turret area
Cp	=	pressure coefficient
C_μ	=	jet momentum coefficient
D	=	turret diameter
f_d	=	actuation frequency
M	=	Mach number
OPD	=	optical path difference
OPD_{rms}	=	root-mean-square of OPD
R	=	turret radius
Re_D	=	Reynolds number

* Research Engineer, AIAA Member.
† Professor, Associate Fellow AIAA.
‡ Assistant Research Professor, AIAA Member.
§ Professor, AIAA Fellow.
** Technical Fellow, Phantom Works, Associate Fellow AIAA.

SR = Strehl ratio
St_D = Strouhal number
U_0 = free stream velocity
U_j = average jet velocity
H = height of turret base
α = azimuthal angle of pressure ports
γ = elevation angle of optical window
γ_s = flow separation angle
ρ = air density

I. Background

Turrets on airborne platforms are bluff-body protrusions that typically consist of a spherical cap supported by a matching cylindrical base. They provide convenient housing for pointing and tracking laser beams from airborne platforms. An optical aperture is therefore built into the turret cap, and can be either flat or conformal. Turrets create wakes that can distort an otherwise planar laser beam[1], even at relatively low subsonic speeds. Consequently, this leads to the laser beam's unsteady defocus and jitter[2].

When an optical wavefront passes through a variable index-of-refraction turbulent flow, its wavefront becomes distorted or aberrated and these distortions are referred to as an aero-optical problem[2]. These wavefront distortions, combined with optical aberrations caused by the wavefront propagation through the atmosphere, known as an atmospheric propagation problem[3], ultimately degrade the light intensity from the otherwise diffraction-limited intensity at the destination. These aberrations have high spatial and temporal bandwidths which are well outside the current control capabilities of traditional adaptive-optics methods[4]. Separated shear layers, such as those in the wakes of bluff bodies, are particularly destructive because of the presence of large coherent vortical structures that are known to be a major source of optical wavefront distortion[5], since they induce strong pressure and density gradients[6]. Left untreated, these shear-layer-related optical aberrations can limit an airborne transmitting system to a forward-looking quadrant only. In order to extend viewing angles to at least a portion of an aft-looking quadrant, a region of the attached flow can be extended by delaying separation of the flow and/or by disrupting formation of the large-scale shear layer vortices. The intent of the work presented in this paper is to evaluate the effectiveness of combined active and passive suppression of the unsteady aerodynamic environment for achieving significant improvement in light transmission efficiency by minimizing laser wavefront degradation. Control of the flow over a bluff-body turret that houses a laser-based optical system must satisfy more demanding requirements than separation control over external aerodynamic surfaces. Whereas the effectiveness of flow control on aerodynamic surfaces can be evaluated in terms of its effect on the time-averaged aerodynamic forces and moments, when the intent of flow control is to enhance transmission of optical wavefronts through regions of separated turbulent flow, spatial and temporal flow dynamics need to be evaluated, rather than just static (mean) effects on the flow.

A flow over a typical turret geometry can be considered as a part of the class of flows over a surface-mounted obstacle having a free end[7]. A common feature of the separated flows behind any of these surface-mounted obstacles is that the resulting separated-flow topology is dominated by three major sources of vorticity: at the juncture of the protuberance and its support surface, over its main body, and at the free end. Furthermore, if the turret's aperture is flat, an additional source of vorticity is introduced at the aperture circumference, unless it has already been fully traversed by the separated flow. The relative contribution of each of these sources depends on the aspect ratio of the obstacle as well as the specifics of the geometry cross-section profile. As the geometry under consideration can be considered a circular cylinder with a modified free end, it is to be expected that the separated flow is dominated by vortices shed off the "free-end" tip (i.e., the hemispherical cap), off the cylinder body, and at the cylinder base. A relative contribution of these three sources clearly depends on the turret's height-to-radius ratio H/R. W hen the support height is commensurate with the turret radius, it is expected that the wake topology would depend on all the sources of vorticity. Having the cap elevated to multiple radii[8] increases the relative importance of the cylindrical support and the wake becomes dominated by vortices shed off the cylindrical support. Conversely, when the support cylinder height is less than the radius, it is expected that shedding of the cylinder body becomes less important. In the limit case, the cylindrical support vanishes completely, and the turret geometry becomes either a hemispherical or spherical shell[9,10]. In such a case, the relative importance between vortices shed off the surface and formed at the juncture depends on the ratio of the incoming boundary layer thickness and the protrusion height. With an increase of this ratio, necklace vortices formed about the juncture between the protrusion and

support surface become more prominent. It should be noted that in Earth flows, it is often observed that the whole protrusion is immersed into the surface boundary layer, but such cases are of less importance for airborne platforms.

Some previous work on flow control of separated flows over bluff-body protrusions has been directly motivated by the aero-optical problems involving an aircraft turret. Passive modifications of the turret geometry were tested by Snyder et al.[11], who considered additions of aft-mounted fairings and splitter plates. They showed reduction of the baseline drag up to 55% by using a large fairing. The separated flow behind the turret with a flat aperture and the effects of passive control on the optical aberrations were also characterized by Gordeyev et al.[12].

Active flow control approaches on turret configurations have been predominantly open-loop in nature. Numerical work by Purhoit et al.[13] predicted significant alteration of the wake structure when investigating low levels of distributed hemisphere suction. Vukasinovic and Glezer[14] demonstrated the effectiveness of fluidic, direct high-frequency control in turbulence suppression behind a bluff-body turret at $Re_D = 8 \cdot 10^5$. Vukasinovic et al.[15] simultaneously measured the aerodynamic and aero-optical environment within the separated flow off a hemispherical turret at free stream Mach-number speeds up to $M = 0.64$. They reported significant suppression of turbulent fluctuations and reduction in optical distortions up to $M = 0.45$ by active flow control.

Renewed interest in the aero-optical problem of the flow over an airborne turret resulted in a number of recent investigations focused on different flow control approaches. Woszidlo, Taubert, and Wygnanski[10] investigated effects of passive generation of streamwise vortices in the oncoming wall boundary layer and active steady suction at the trailing-edge base on separation of the low-speed flow over the spherical protuberances. The former delayed separation off the surface, while the latter was able to remove necklace vortices around the protuberance and thereby eliminate one source of vorticity and turbulence intensity in the wake. The effectiveness of direct, small-scale control ($St_D > 10$) of the separated flow over a hemispherical protuberance with a thin upstream boundary layer was demonstrated by Vukasinovic, Brzozowski, and Glezer[9] at $Re_D = 4 - 7 \cdot 10^5$. They showed that the presence of flow control can substantially reduce the extent of the recirculating domain downstream of the hemisphere with significant reduction in turbulent kinetic energy. Numerical work of Morgan and Visbal[16] emphasized that distributed porous suction over forward turret surface significantly delayed separation off the hemisphere at $M = 0.4$ and consequently reduced the wake extent and its turbulent intensity. Vukasinovic et al.[17] and Gordeyev et al.[18] measured both aerodynamic and aero-optical effects of synthetic jet active control of the flow over a turret, nominally at $M = 0.3$ and $Re_D = 4.5 \cdot 10^6$. It was shown that aerodynamic improvements in separation delay and suppression of turbulent energy within the wake resulted in about 30% suppression in optical aberrations as measured directly by the Malley probe. Besides the above-mentioned open-loop control approaches, Wallace et al.[19] also presented some examples of closed-loop control effects based on the feedback from the dynamic pressure sensors over the flat aperture. Finally, Gordeyev and Jumper[20] reviewed past work on the baseline and controlled flow over an airborne turret.

The present investigation builds on the findings of previous work on active control of flow over a turret by direct small-scale excitation of the flow by arrays of surface-mounted synthetic jets[17,18]. Although actuation at the frequencies comparable with the natural wake frequencies is often used in the applications aimed at a flow separation delay over aerodynamic surfaces, there is reason to believe that excitation of the large-scale, organized motions in the wake by such a control could induce even higher optical aberrations[5] in spite of a possible favorable effect in the static (mean) sense. Therefore, actuation at the scales substantially smaller than the wake natural scales is selected, since suppression of the organized large-scale structures in the flow under such a control has already proven effective in the planar shear layers[21,22,23]. Besides active flow control, the present work utilizes favorable global flow alterations induced by simple passive modifications of the base turret geometry. Favorable effects that are primarily manifested through the flow separation delay via passive control are further augmented by active actuation. Simultaneous active and passive control comprise hybrid control that results in concomitant delay of flow separation and active, dissipative suppression of turbulent motions within the separated shear layer. It is interesting to note that one of the first turret flow control approaches proposed in the literature[24] is also hybrid in nature according to the definition above, as it proposed a combination of a long aft fairing (passive) and dual suction (active) control at the support surface, integrated into the fairing. While the primary objective of the current work is to assess the effectiveness of hybrid flow control for suppression of optical aberrations at $M = 0.3$, the control effectiveness was further characterized at $M = 0.4$ and 0.5. While the primary focus of this paper is on the aerodynamic effects of active and hybrid flow control, the accompanying direct aero-optical characterization is discussed in great detail in the companion paper[25]. The experimental setup and procedure are described in Section II. The characterization of the base flow is described in Section III; Sections IV and V present the results of active and hybrid control, respectively. Finally, the conclusions are presented in Section VI.

II. Experimental Setup and Procedures

All experiments were conducted at the Subsonic Aerodynamic Research Laboratory (SARL) facility at Wright-Patterson Air Force Base. The SARL facility has an open-loop indraft wind tunnel with a 2.13 × 3.05 m octagonal test section that is 4.57 m long. Mach number can be varied between 0.1 and 0.5. The test section was designed for a maximal optical access, having twenty eight windows built into the test section walls, and they comprise 56 percent of the test section surface area. The tunnel has a 14 × 15.2 m inlet, giving a 35:1 contraction ratio. Honeycomb and screens are installed in the inlet before the contraction for turbulence intensity management. The primary test section speed for the current tests was $M = 0.3$, while additional tests were run at $M = 0.4$ and 0.5, which correspond to Reynolds numbers $Re_D = 4.4 \cdot 10^6 - 7.4 \cdot 10^6$. The turret model mounted onto the side wall of the test section is shown in Figure 1*a*. It measures 0.61 m in diameter, and is equipped with a 0.254 m diameter spherical cap that models an optical window and therefore the aperture area is unavailable for the flow control hardware. During the aero-optical portion of the test[25], the instrumented cap was replaced by a full optical window with a mirror underneath. The actual laser beam reflecting out of the optical window is visualized in Figure 1*b*.

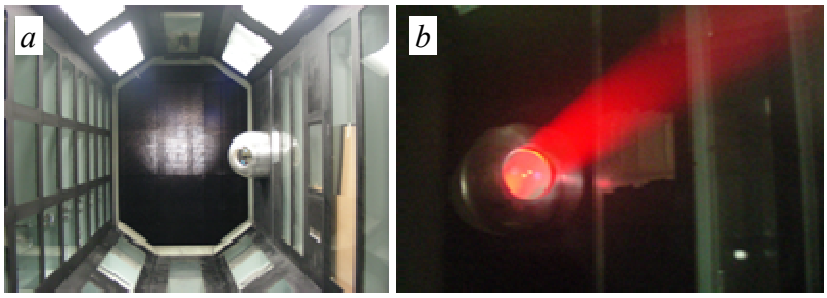

Figure 1. *Turret model in the SARL tunnel (a) and the 25.4 cm dia. optical beam reflecting out of the turret (b).*

A nominal turret model, shown schematically in Figure 2*a-b,* is a modified turret model previously used by Vukasinovic et al.[17]. The cylindrical turret base ($H/R = 0.6$) is stationary, but the central hemispherical top ($R = 0.305$ m) is fully rotational about the z-axis in the turret's zenith plane, thus allowing variation in the window's elevation angle γ, which is defined as the central angular position of the window's center, relative to the horizon (free stream flow). The spherical top is instrumented with static pressure ports that are distributed along the central, middle (20° off centerline), and the outer (40° off centerline) planes, which include 39, 44, and 39 ports, respectively. In addition to these main pressure ports, nine static pressure ports are also distributed just upstream from the optical window, such that the middle port is in the central plane, and four pressure ports are distributed over each half of the window, having azimuthal angles $\alpha = 12.5°$, 25.6°, 39.7°, and 57.7°. These additional nine ports are used to assess the flow symmetry and spanwise (z-direction) effects of the actuation. Static pressure measurements were acquired using a Pressure Systems scanner, where average pressure measurements are typically measured over five hundred individual samples. Two main modifications of the previous turret model[17] are addition of passive flow control elements (partition plates) and surface

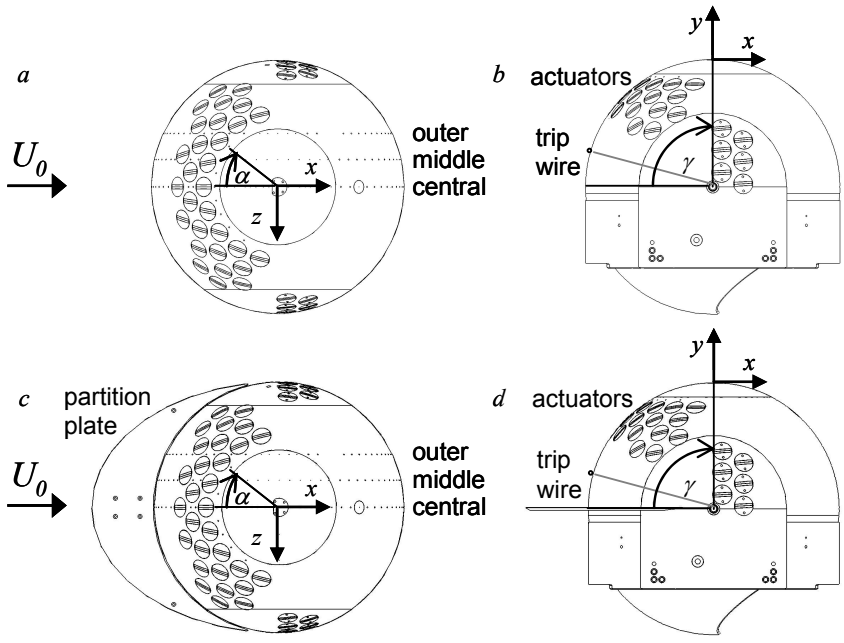

Figure 2. *Top (a,c) and side (b,d) views of the 0.61 m dia. turret model having a 0.254 m instrumented spherical cap in place of an optical window for the nominal (a,b) and modified (c,d) turret geometry.*

redistribution of the active control sources. The former was motivated by the findings of active flow control of the separated flow off the hemispherical protuberance (i.e., a turret with no cylinder support)[9,15]. The latter was motivated by the findings of Vukasinovic et al.[17] that the farthest-downstream actuators that were wrapped around the optical window did not improve the aerodynamic and optical environment behind the turret. Therefore, six of those far-end actuators on each window side were redistributed to the stationary side of the turret, i.e., trunnions, as shown in Figures 2*a*-*b*. The other 30 actuators were distributed in multiple rows, just upstream from the optical window, preserving the same pattern as in the previous tests. Furthermore, governed by the previous results, the current tests were done with the actuators injecting predominantly streamwise vorticity into the flow. Hence, a total of 42 individually-addressable actuator modules were distributed over the turret surface. Each actuator module has a high aspect ratio rectangular jet orifice (measuring 38.1 × 0.5 mm). Besides the actuator design, the accompanying amplifier circuitry for the actuators was also designed and built at Georgia Tech. It should be noted that no independent repositioning of the actuators relative to the optical window is allowed, as the whole hemispherical top rotates as a rigid body. This real-application requirement prompted distribution of the actuators in multiple rows, as the relative distance from the control input to the local flow separation point varies proportionally to the turret rotation. As mentioned above, a major change in the turret geometry was done by addition of forward partition plates at the interface of the hemisphere and the supporting cylinder. Schematics of the modified turret geometry with a $R/2$ long partition plate is shown in Figure 2*c*-*d*. This passive modification of the turret geometry was motivated by a desire to effect suppression of interaction between the hemisphere and cylinder wakes, as well as by generation of frontal necklace vortices that were expected to have a favorable effect on bringing the high-momentum fluid from the outer flow closer to the central zone of the turret surface. Two passive modifications of the base turret geometry were tested: the addition of forward partition plates of lengths $R/2$ and R at the point of mating of the hemisphere and the cylinder. In the present experiments, the actuation frequency was kept at f_d = 1,600 Hz, while the actuation strength was varied over $3 \cdot 10^{-6} < C_\mu < 1.5 \cdot 10^{-5}$ per single active actuator, where the jet momentum coefficient is defined as $C_\mu = \rho U_j^2 A_j / (\rho U_0^2 A_o)$, where A_j is the total jet orifice area, A_o is the frontal projection of the turret, and U_j is the average jet velocity during the expulsion part of the cycle. It should be noted that full control utilizing all the available actuators corresponds to the jet momentum coefficient of $C_\mu = 6.5 \bullet 10^{-4}$ at $M = 0.3$, which is the flow condition of primary interest.

Spectral characterization of the baseline (non-actuated) and actuated flows was accomplished using single-sensor hot film anemometry. For that purpose, three hot-film probes were mounted on retractable holders and stowed in surface wall depressions when not in use. During the measurements, only one probe at a time was elevated from the surface and positioned at the measurement location. The sensor streamwise positions are x/R = 0.5 (HW1), 1.1 (HW2), and 1.5 (HW3), where x is measured from the hemisphere center (Figure 2). All the measurement locations are shown in Figure 3, where the multiple cross-stream measurement locations were selected so that the local shear layer thickness was traversed. Hot-film output signal was sampled at 30 kHz so that the measurement resolution was about 1.8 Hz in the frequency domain. For a given flow condition, an averaged power spectrum was composed of fifty individual power spectra for suppression of random noise.

Additional flow characterization was done by oil-flow visualization, which was used to gain a better understanding of the global baseline flow topology. The oil was applied so as to capture the flow footprint at the turret support wall, accompanied by partial visualization of the flow on the turret surface and the partition plates (when present). The main captured features included the front and back stagnation points, a horseshoe vortex pattern that originates upstream of the cylindrical support, the main wake formed by the flow separation off the hemispherical top, secondary separation zones off the cylindrical support, and a partial separation line on the hemispherical top. All these features are combined into a single schematic representation of the flow footprint for each baseline flow field.

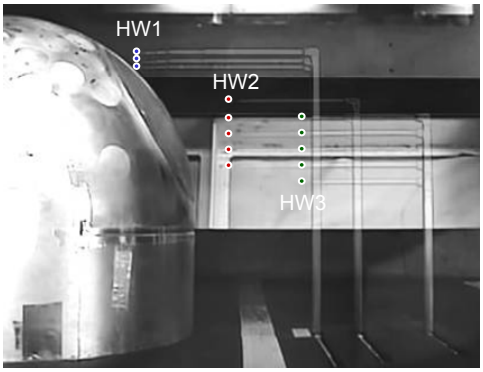

Figure 3. *Overlapped measurement positions of the three hot-film sensors downstream from the turret.*

III. The Baseline Flow

Earlier investigations[15,17] have demonstrated that the topology of the baseline turret flow is rather complex and Mach and Reynolds number dependent. In order to avoid changes in separation that are associated with flow transition over the model smooth surface, the hemisphere's boundary layer in the present experiments was tripped using an overall 0.3 mm dia. wire that was placed along meridional plane at a 15° elevation relative to the center (symmetry) plane of the turret.

The resulting baseline flows are first characterized using measurements of static pressure distributions in the central, middle and outer planes (Figure 2). The pressure profiles in these three planes are shown in Figure 4 for window elevation angles $\gamma = 139°$, 145°, and 150°, and $M = 0.3$, 0.4, and 0.5. The baseline profiles for the same turret geometry[17] for $\gamma = 129°$, 137°, 143°, and 148°, and $M = 0.3$, 0.4, and 0.5 are included in the same figure. An excellent agreement between the current and previous measurement indicates invariant baseline flow conditions, which suggest that, for a given Mach number, the flow separates first over the outer edges of the optical window and remains attached farthest in the central plane, as the separation angles in each measurement plane nearly coincide in its own reference angles. The pressure profiles shown in Figure 4 also indicate that the separation angle in all three planes shifts slightly upstream with increasing M, such that the flow separates just upstream from 120° in the central plane at $M = 0.3$, while at $M = 0.5$, the separation point is at about $\gamma_s = 115°$. It should be noted that the baseline flow in the center zone over the hemispherical cap does not differ significantly from the flow over the upper half of the full sphere immersed into the same outer flow. Given the Reynolds number greater than 10^6 in the present experiments, the flow separation for an equivalent full sphere occurs in the supercritical regime where the boundary layer over the hemisphere is fully turbulent at the point of separation. According to Achenbach[26], the separation angle in the central plane should therefore be between 115° and 120°. Clearly, the present results for the turret with conformal aperture are in good agreement with the analogous results for the full sphere. An insight into the flow condition just upstream from the optical window is gained by the static pressure distributions over nine symmetry ports distributed along the window's upstream edge (Figure 2). These baseline pressure distributions are shown in Figure 5 for both the current and previous[17] tests at $M = 0.3$, and their pressure port positions comprise a full span of elevation angles of the most interest, $\gamma = 120° - 150°$, and also serve as a check for consistent baseline flow conditions in both tests. Besides a close agreement between the tests results[17] at $\gamma = 129°$ and 150°, and the current $\gamma = 130°$ and 150°, it is also indicative that the flow starts to separate at the outer upstream edges of the window at about $\gamma = 135°$, and that past $\gamma = 143°$ the baseline flow becomes almost fully separated over the whole optical window.

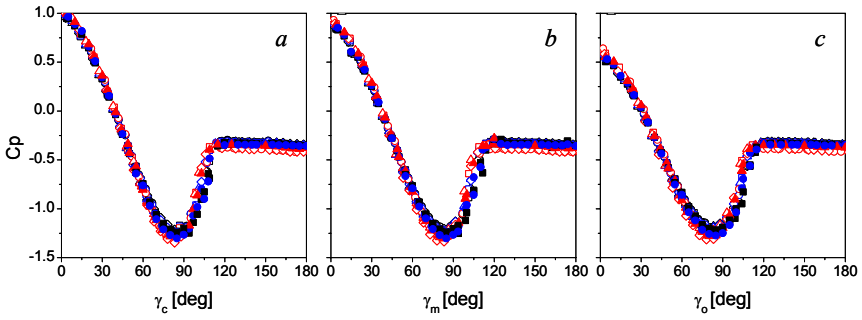

Figure 4. *Overlapped static pressure measurements at window elevation angles γ = 129°, 137°, 143°, and 148° (open symbols)[17], and γ = 139°, 145°, and 150° (solid symbols), for the baseline flows at M = 0.3 (—), 0.4 (—), and 0.5 (—) in the central (a), middle (b), and the outer (c) plane.*

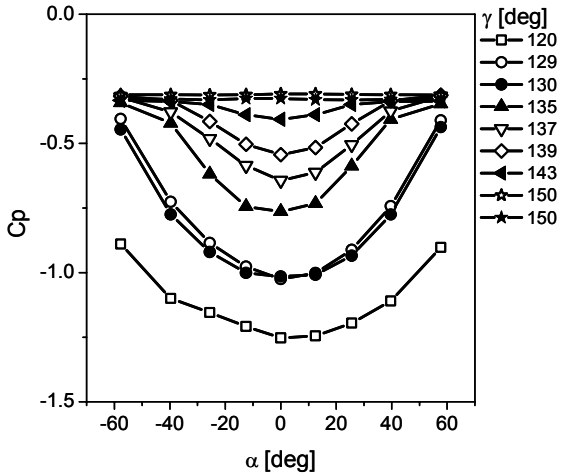

Figure 5. *Static pressure profiles upstream from the optical window for a range of turret elevation angles γ = 120° – 150° and M = 0.3 for the current (solid symbols) and previous[17] (open symbols) tests.*

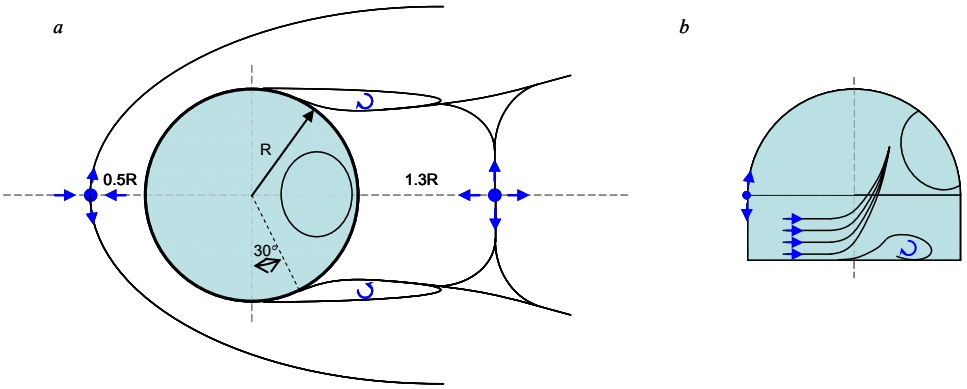

Figure 6. *Schematics of the surface oil-flow visualization of the baseline flow at M = 0.3 at the support wall (a) and turret surface (b) for the nominal turret geometry.*

Next, the global topology of the baseline flow at $M = 0.3$ was investigated using surface oil-flow visualization. The main footprint of the flow was visualized over the flat surface of the supporting turret wall, and additional visualization was performed along the cylindrical turret base. The recorded images of the surface oil visualization showed that the baseline flow over the turret is quite symmetric. Some features of the flow that were educed from these images are shown schematically in Figures 6*a* (the turret support plane) and 6*b* (the cylinder surface). As the oncoming boundary layer approaches the adverse pressure gradient induced by the presence of the cylinder support, a spanwise (necklace) vortex is formed which becomes strained and deformed under the modified pressure field, giving a rise to the streamwise vortex branches along each spanwise edge of the cylinder. A stagnation point is formed at $0.5R$ upstream from the turret edge, and the outer flow is displaced by the bluff body, accelerates over the hemisphere surface and around the cylindrical surface until the adverse pressure gradients on the aft sides induce separation. The flow footprints shown schematically in Figure 6*a* indicate that the flow separates off the cylinder base near its apex, and spreads azimuthally by approximately 120°. The visualization on the surface of the cylinder in Figure 6*b* indicates the 3D nature of the separating flow near the cylinder base, as well as its localized, near-wall effect. Further away from the support wall, the flow trajectories over the cylinder become displaced towards the hemispherical turret cap, and merge into a separation line. This visualization supports the assessment, based on the static pressure measurements (Figure 4), that the flow separates first at the spanwise edges of the turret and remains attached farthest in the (center) plane of symmetry. The ensuing separated flow off the turret surface has a main central wake that reattaches to the support wall at approximately $1.3R$ downstream from the turret edge, and two additional near-wall vertical traces that are associated with the vortices shed off the juncture between the cylinder and the support wall. After initial narrowing, the main wake begins to spread as shown in Figure 6*a*. These visualizations indicate that the overall wake dynamics is dominated by the flow separation off the hemispherical cap, while the separation at the cylinder base has a rather localized effect on the main wake. In contrast to these findings, measurements in a high aspect ratio turret flow[8], where the cylindrical base is much taller than its radius, show that the near wake is dominated by the dynamics of the vortices shed off the supporting cylinder.

Spectral characterization of separated flows behind the turret was done by hot-film anemometry, as described in Section II. While major spectral characterization of the separated flow was done in connection with the evaluation of the flow control approaches, the baseline flow was first analyzed from the standpoint of invariant flow dynamics at different elevation angles of the turret. An example of these data at $M = 0.3$ is shown in Figure 7, which includes three

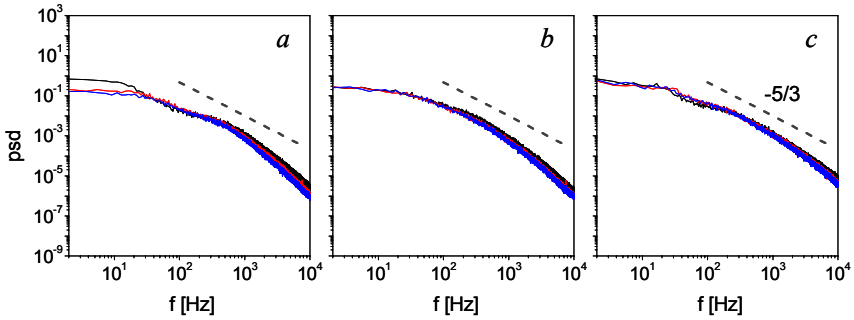

Figure 7. *Power spectra of the baseline velocity fluctuations at M = 0.3 and γ = 139° (—), 145° (—), and 150° (—) measured at the shear layer centre at HW1 (a), HW2 (b), and HW3 (c) locations.*

spectra of velocity fluctuations measured at x/R = 0.5 (HW1), 1.1 (HW2), and 1.5 (HW3) at the fixed position within the shear layer, and for three elevation angles γ = 139°, 145°, and 150°. These data confirm that there is no significant difference among the baseline flows, as the baseline flow dynamics should be independent of the turret elevation angle. Some variation of energy distributions that is detected at the closest measurement station (Figure 7*a*) is attributed to an error associated with the positioning of the hot-film sensor within the narrow shear layer, as it is in the case of the starting shear layer. Figure 7 also demonstrates how the inertial range of scales shifts towards the higher frequencies with an increase in downstream distance, as turbulent evolution of the flow generates motions of decreasing scales.

IV. Active Flow Control

Figure 8 shows static pressure distributions over three measured planes (central, middle, and outer, Figure 2) for the baseline and controlled flows at M = 0.3, 0.4, and 0.5. As flow control is activated, there is an almost identical effect measured in all three planes at γ = 139° (Figures 8*a-c*). The flow separation becomes delayed by $\Delta\gamma_s$ > 10° and, contrary to previous tests[17], this effect does not weaken across the span. Such extended effect in the spanwise direction relative to the previous tests[17] is attributed to the spatial redistribution of actuators, which also populate the turret sides in the present tests (Figure 2*c-d*). As the Mach number is increased to M = 0.4 (Figures 8*d-f*), a substantial separation delay is sustained upon actuation in the central plane, with some weakening towards the outer planes. Finally, at the highest Mach number M = 0.5 (Figures 8*g-i*), nearly-uniform but weak separation delay is achieved across the optical window area. Overall, redistribution of the control actuators to the turret sides showed consistent improvement in separation delay, when compared to the previous test[17]. These findings are also in accord with the conclusions drawn from the turret control at lower speeds[14], which explored the effect of varying spanwise extent of the control sources.

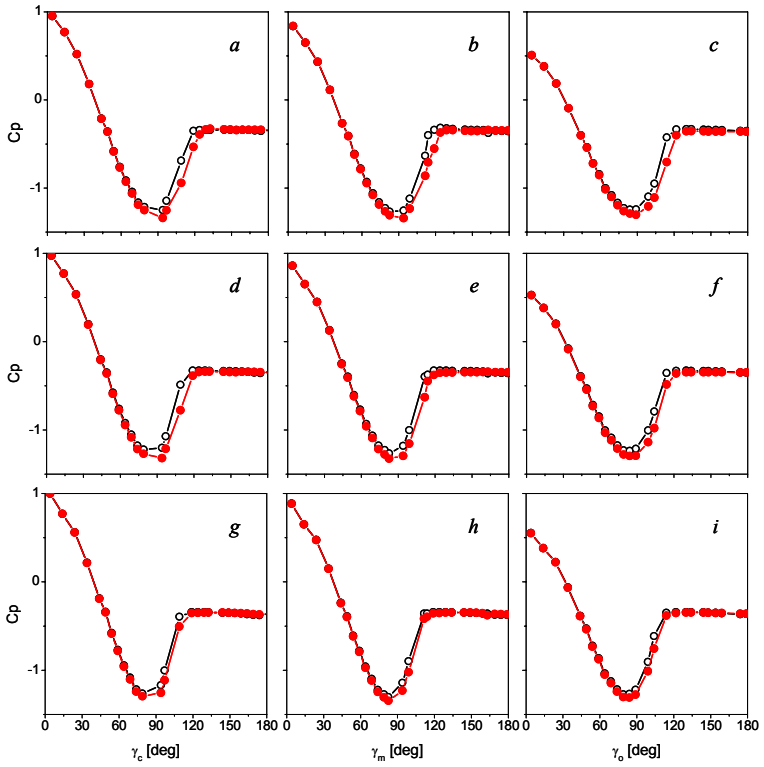

Figure 8. *Static baseline pressure profiles at the window elevation angle γ = 139° and M = 0.3 (a – c), 0.4 (d – f), and 0.5 (g – i) in the central (a, d, g), middle (b, e, h), and the outer (c, f, i) planes for the baseline (○) and the flow actuated by full actuation (●).*

Static pressure distributions just upstream of the optical window edge are shown in Figure 9, corresponding to the test cases of Figure 8. Regardless of the Mach number, the shape of any baseline pressure distribution clearly indicates that the flow separates first at the outer edges of the optical window, and that the upstream central zone of the window is traversed by the still-attached flow. As flow control is activated, significant acceleration of flow around the turret is induced, manifested by a pressure drop

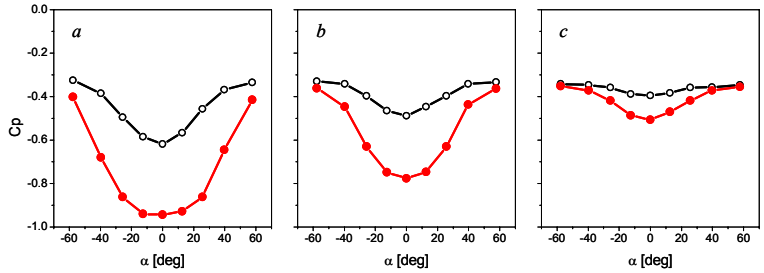

Figure 9. *Pressure distributions about the optical window center (α = 0°) at window elevation angle γ = 139° for the baseline flow (○) and the actuated (●) flow at M = 0.3 (a) and 0.4 (b), and 0.5 (c).*

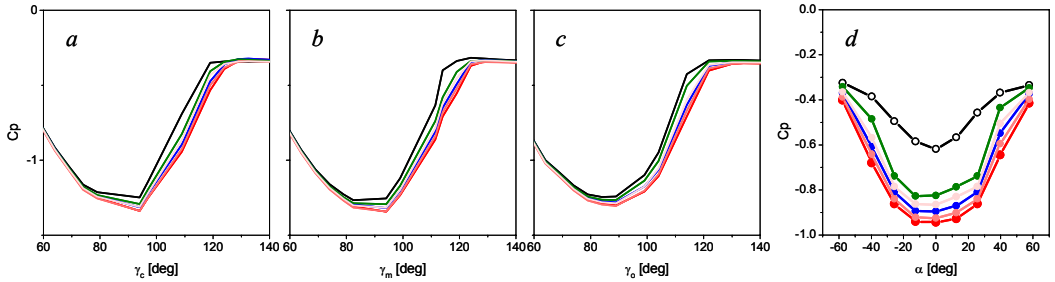

Figure 10. *Static pressure profiles in the central (a), middle (b), and outer (c) planes for the baseline (—) and actuated flows at M = 0.3 and γ = 139°, by ACT1 (—), ACT2 (—), ACT3 (—), ACT4 (—), and ACT5 (—). Corresponding pressure distributions around the optical window are shown in (d).*

across the window upstream edge. Consequently, this effect enables flow to remain attached further in the streamwise direction. This favorable effect on flow separation is pronounced strongly in the central zone of the optical window, with some weakening in the outward direction. It should be noted that comparable results from previous tests[17] showed that favorable effect of flow control completely vanished at the outer edges of the window ($\alpha \approx \pm 60°$). However, the current results show that there is still a notable effect across the span, which is attributed to redistribution of the actuators and their presence along the cylinder sides, which is known to enhance the overall flow control effect[14]. Furthermore, it appears that the current flow control approach also enhances separation delay across all Mach numbers tested, when compared to the previous tests[17].

Besides the nominal actuation approach where all of the jets are utilized at the highest jet momentum coefficient (case AC1), additional tests were done to test how different spatial distributions of actuators affect the flow control and how varying jet momentum coefficient affects the flow control effectiveness. The former is done by rendering two side clusters of actuators inactive (AC2), see Figure 2, and by the flow control exclusively by the band of actuators closest to the optical window (AC3). The next test was facilitated by a full set of actuators having the actuator strength lowered below the nominal level (AC4), and lowered even further (AC5). Static pressure profiles corresponding to the baseline flow at $\gamma = 139°$ and these five actuation scenarios are shown in Figures 10*a-c* for the central, middle, and the outer measurement planes, respectively. As seen in these plots, separation delay is directly proportional to both the actuation strength and population of the actuation sources. These results are in accord with previous similar tests on similar geometries[14,17]. Based on the profiles that result from the actuation cases AC1-3, it can be concluded that exclusion of side actuators has a less detrimental effect on flow separation delay than exclusion of the second row of actuators upstream from the optical window. The weakening of separation delay with weakening of the jet strength has already been proven in both low-speed[14] and high-speed[15] tests, and current results support those findings. It is interesting

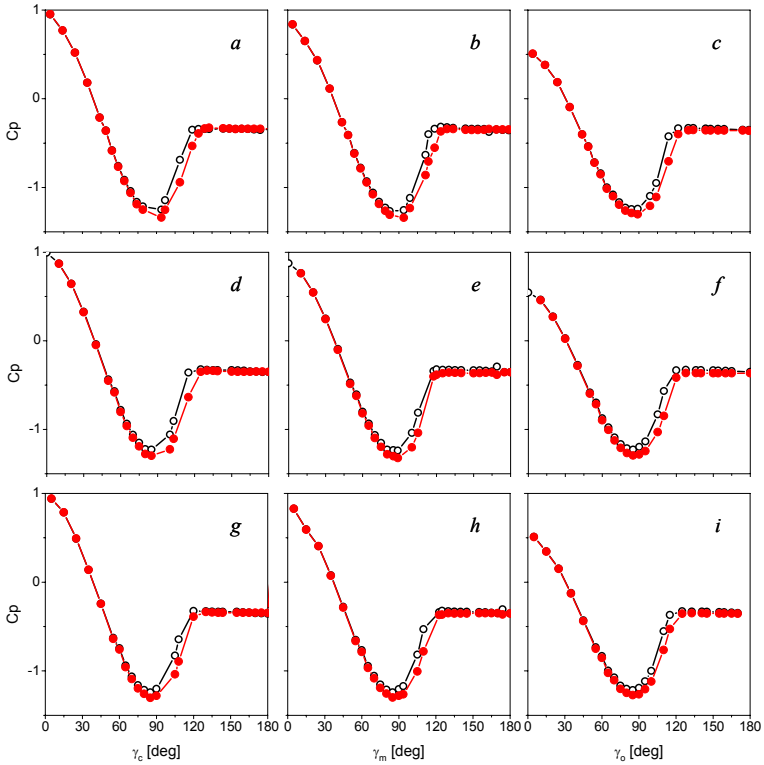

Figure 11. *Static baseline pressure profiles at M = 0.3 and γ = 139° (a – c), 145° (d – f), and 150° (g – i) in the central (a, d, g), middle (b, e, h), and the outer (c, f, i) planes for the baseline (○) and the flow actuated by full actuation (●).*

to note, however, that the weakest actuation at the full set of actuators (AC5) is still preferable than actuation at full strength by a significantly-reduced number of actuators (AC3). Accompanying static pressure distributions over the front border of the optical window are shown in Figure 10*d*, and these profiles suggest that the principal effects seen in the three representative planes (Figures 10*a-c*) are a true representative of the full spanwise effects over the optical window, since a family of inverted bell-shaped profiles follow the same trends discussed in conjunction with Figures 10*a-c*.

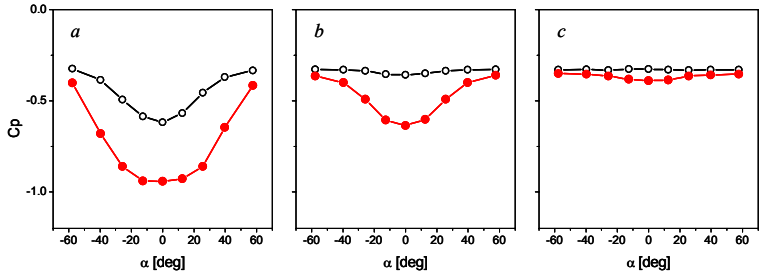

Figure 12. *Pressure distributions about the optical window center (α = 0°) at M = 0.3 and window elevation angle γ = 139° (a), 145° (b) and 150° (c) for the baseline flow (○) at the actuated (●) flow.*

Next, the use of active flow control was tested at three turret elevation angles, γ = 139°, 145°, and 150°, and M = 0.3. Resulting static pressure profiles measured in three planes: central (symmetry plane), middle (20°-off central), and outer (40°-off central) are shown in Figure 11 for the baseline flow (open symbols) and controlled flow by the full set of actuators (solid symbols). Baseline profiles indicate, as expected, a stagnation point (Cp = 1) at zero incidence in the central plane and non-zero, increasing velocities towards the outer plane (Cp < 1). Also, as the flow accelerates towards the turret apex, local velocities there ($\gamma_{c,m,o}$ = 90°) are nearly identical. The effects of the flow control at γ = 139° are already discussed in conjunction with Figure 8. The strong separation delay seen at this elevation angle (Figures 11*a-c*) is sustained at γ = 145° (Figures 11*d-f*), while a somewhat smaller separation delay is measured at the highest elevation angle γ = 150° (Figures 11*g-i*). Overall, the separation delay indicates that the flow control effect in the present tests has more favorable effect on mitigation of flow separation over the optical window than in the previous test[17], which is attributed to redistribution of ineffective control elements to the turret sides, thus effectively increasing the spanwise extent of control elements.

Further analysis of the control effect is based on the static pressure distributions just upstream of the optical window, which are shown in Figure 12, corresponding to the test cases of Figure 11. As already discussed with respect to Figure 9, the shape of the baseline pressure distribution at γ = 139° (Figure 12*a*) clearly indicates that the flow separates first at the outer edges of the optical window, and that the upstream central zone of the window is traversed by the still attached flow. As the flow control is activated, a favorable effect of the flow separation delay is pronounced strongly in the central zone of the optical

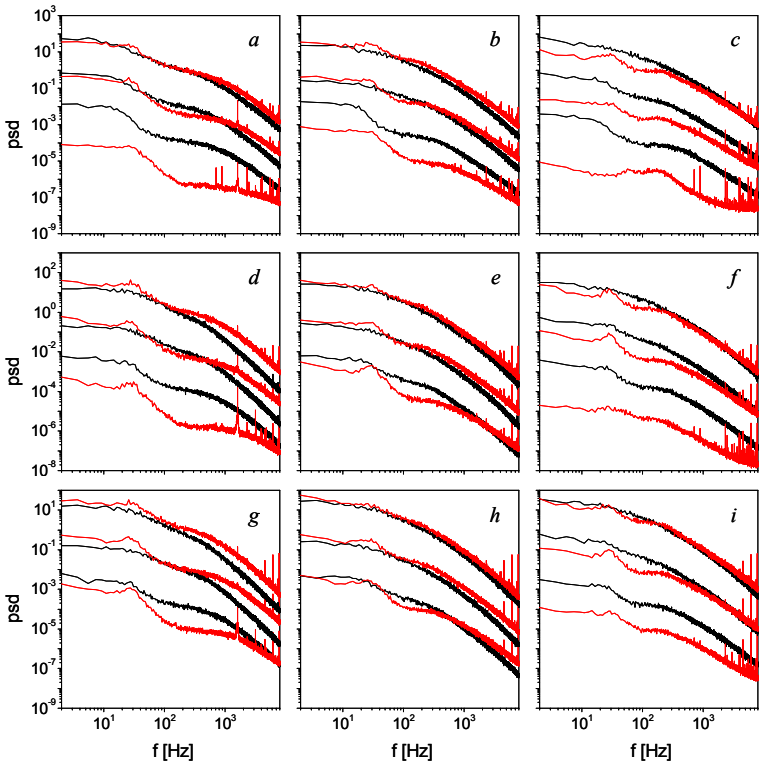

Figure 13. *Power spectra of the velocity fluctuations (M = 0.3) for the baseline (—) and actuated flow (—) at γ = 139° (a,b,c), 145° (d,e,f), and 150° (g,h,i), measured by the HW1 (a,d,g), HW2 (b,e,h), and HW3 (c,f,i) at the high-speed edge (lowest pair), middle (middle pair) and low-speed edge (highest pair) of the shear layer. Pairs of spectra for the middle and low-speed edge are offset by two and four decades, respectively.*

window, with some weakening in the outward direction. At the next elevation angle, $\gamma = 145°$ (Figure 12*b*), the flow is almost fully separated at the measurement locations upstream from the optical window. Upon the activation of flow control, the non-separated flow condition is recovered upstream from the window border, as evidenced by the pressure dip. The inverted bell shape suggests again that the control effect is strongest at the central zone of the window, and that it weakens in the outward direction. Still, some effect is seen again even in the most-outward measurement location, which was not the case in the previous active control tests[17]. The baseline flow is fully separated at the highest elevation angle $\gamma = 150°$ (Figure 12*c*), and that appears to be the most difficult case for maintaining the non-separated flow over at least part of the optical window. The flow control still improves the flow state, but recovers only a nearly-separated flow condition upstream from the window. Overall trends in the results of the flow control measured in the current tests are in accord with the previous tests, at both low-speed[14] and high-speed[15] tunnel speeds, and they suggest that optimal flow control source positioning is just upstream from the local separation. However, application-oriented distribution of control sources limited a real estate available for the distribution of actuators. Furthermore, their continuous rotation relative to the separation line with rotation of the optical window results in a more preferable relative positioning of the actuators at lower elevation angles γ, and less preferable relative positioning of the actuators at higher elevation angles.

Besides a static (mean) flow control effect on the base turret geometry that was discussed above, characterization of the flow dynamics was done in the spectral domain using the single-sensor hot-film anemometry. Hot-film measurements were done at three downstream locations HW1, HW2, and HW3, as described in Section II. As an illustration of flow control effect on the shear layer, velocity fluctuation spectra are shown for the baseline and the actuated flows in Figure 13 for $M = 0.3$ and $\gamma = 139°$, 145°, and 150°. Three power spectra for the baseline and actuated flows are shown for each γ and at each downstream measurement position, where the bottom pair of spectra corresponds to the high-speed edge of the shear layer, the middle pair corresponds to the shear layer bulk (and is offset by 10^2 in magnitude for clarity), and the upper pair corresponds to the low-speed edge of the shear layer (and is offset by 10^4 in magnitude for clarity). Similar effects are seen at all elevation angles. A typical near-field effect of actuation is seen at both HW1 (Figures 13*a*,*d*,*g*) and HW2 (Figures 13*b*,*e*,*h*) positions: significant broadband reduction in fluctuating energy is measured over the high-speed edge of the shear layer, and increase of the energy at small scales and concomitant decrease of energy at the large scales is detected within the shear layer bulk. Furthermore, predominantly an increase in energy is detected along the low-speed edge of the shear layer. At the farthest downstream measurement location (Figures 13*c*,*f*,*i*), suppression of energy over the large-scale motions dominates each spectra, regardless of the elevation angle. Also, as the control sources are moved downstream with the increase in elevation angle, some increase in energy of the small scales becomes prominent with an increase in γ.

V. Hybrid Flow Control

Hybrid flow control applied in this work is comprised of passive flow control by addition of a forward partition plate to the base turret geometry in addition to the active flow control that is already described in Section IV. A motivation for addition of the forward partition plate came from the previous flow control tests on the hemispherical turret, i.e., a hemispherical shell on a horizontal support wall[9]. The main flow feature present in a baseline flow over the hemispherical, but not in the hemisphere-on-cylinder turret, is a formation of the necklace vortices at the front stagnation zone of the hemisphere. These necklace vortices have a potential twofold favorable effect on the flow separation delay: they effectively displace the stagnation point downstream from the horizon, and have a predominantly downwash motion towards the hemisphere centre. They also have a potentially detrimental effect on turbulence intensity in the wake, because they constitute an additional vorticity source that merges with the main wake. Therefore, addition of the forward partition plate is designed to emulate a presence of the support wall, as in the hemispherical turret geometry. To test this approach, two passive modifications of the base turret geometry were tested: the addition of a 15.2 cm and 30.4 cm long forward partition plates at the point of mating of the hemisphere and the cylinder. The resulting modified turret geometries are shown in Figure 14. It should be noted that addition of

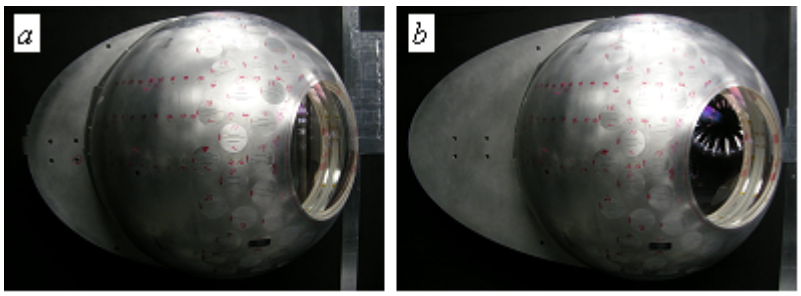

Figure 14. *Passive modifications of the base turret geometry by addition of the forward short (a) and long (b) partition plate.*

an aft partition plate was also tested in low-speed tests[14], in which case the plate's role is shifted, acting as a splitter between the wakes forming off the hemisphere and off the cylindrical support.

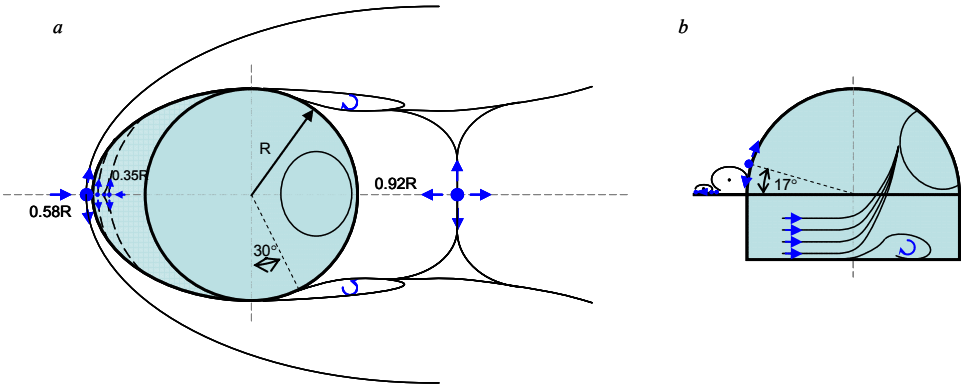

Figure 15. *Schematics of the surface oil-flow visualization of the baseline flow at M = 0.3 at the support wall (a) and turret surface (b) for the turret with a short forward partition plate.*

First, the resulting baseline flows (without the active flow control) are characterized in order to gain a better understanding of the impact that only a passive control surfaces have on the ensuing separated flow. Altered global flow topology is assessed from the surface oil-flow visualization, which is already presented for the base turret geometry (no passive modifications) in Figure 6. Significant impact on the flow topology is seen in Figure 15, when the shorter forward partition plate is added to the base turret geometry. Two major differences are seen relative to the baseline topology at $M = 0.3$ (Figure 6). First, the flow remains attached farther over the hemispherical surface, i.e., the separation line is pushed downstream (Figure 15*b*), such that the flow remains attached over the most upstream portion of the optical window. Second, once separated, the flow reattaches to the support wall closer to the model, at about $0.92R$ downstream from the model edge. Secondary separation off the cylinder base becomes altered too, as the main separated zone spreads even more across the span, and measures $1.83R$ at its throat. A presence of the plate also clearly modifies the initial interaction region between the oncoming flow and the turret. The wall stagnation point becomes displaced farther upstream at $0.58R$, while the major alteration is observed at the front stagnation region at the turret surface (Figure 15*a*). Presumably due to the finite plate thickness, the flow separates off the leading edge of the plate, and as soon as it reattaches to the plate it separates again at about $0.35R$ upstream from the hemisphere due to the modified pressure by the hemispherical body. This modified stagnation zone in front of the hemispherical cap displaces the stagnation point on the body to about 17° relative to the horizon (Figure 15*b*), and creates a recirculating zone that eventually opens around the body. As the outer speed increases to $M = 0.4$ (not shown), all major features described above for $M = 0.3$ are present, with some length-scale alterations: the necklace vortices around the hemispherical cap become narrower, i.e., spread about $0.31R$ upstream from the cap, while the reattachment point of the wake moves even closer to the turret at $0.83R$ downstream from the turret edge. As already stated, the baseline wake over the nominal turret geometry at $M = 0.4$ reattaches at $1.92R$. Hence, addition of the shorter forward plate results in over a 50% reduction in the wake length. Note that the corresponding

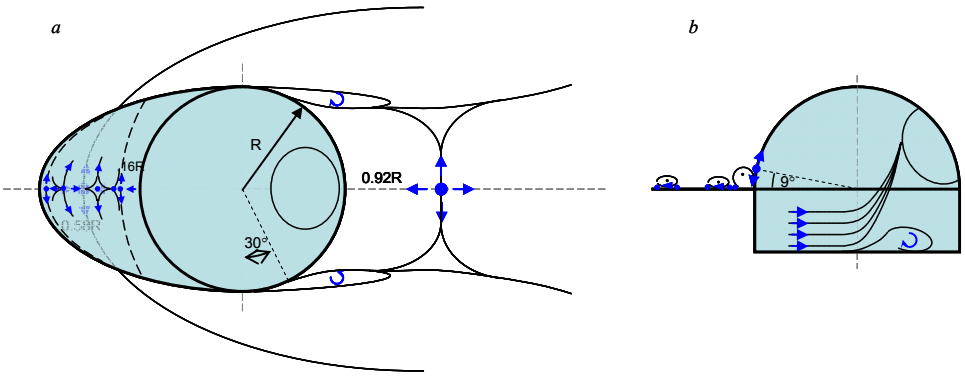

Figure 16. *Schematics of the surface oil-flow visualization of the baseline flow at M = 0.3 at the support wall (a) and turret surface (b) for the turret with a long forward partition plate.*

reduction in the wake extent is about 30% at M = 0.3, i.e., a higher wake suppression is achieved at higher Mach number.

A global flow topology does not change much at M = 0.3 if a longer partition plate is placed instead of the shorter one, as seen in the schematics shown in Figure 16. Virtually nothing changes besides the approach stagnation zone to the hemispherical surface. The longer plate enables a fuller flow evolution over its surface, once the approaching flow separates off the leading edge of the plate. The flow first reattaches to the plate surface, and then forms a double stagnation zone in front of the hemispherical cap, similar to the double front stagnation at the support wall for the base turret geometry at M = 0.4. The inner recirculating zone measures about 0.16R in the central cross section (less than the corresponding one at the short plate) and opens around the hemispherical cap. As a consequence, the stagnation point at the hemispherical surface is now less displaced relative to its displacement with the shorter plate, to about 9° (Figure 16*b*). As the outer speed is increased to M = 0.4 (not shown), the central reattachment point of the wake becomes slightly pushed downstream to about 1.04R, which represents more than a 45% reduction of the wake length than in the corresponding baseline flow over the nominal turret geometry (without any partition plate).

Similar effects of both partition plates on the baseline flow are also seen in the static pressure profiles along the central, middle, and outer measurement planes. Figure 17 shows these profiles for the base turret geometry and passive modifications including both partition plates at γ = 139° and M = 0.3, 0.4, and 0.5. Regardless of the pressure plane or even a Mach number, a significant favorable alteration of the baseline flow around the turret is measured after the addition of either splitter plate. This alteration of the baseline flow is primarily manifested through significant separation delay of more than ten degrees in any of the measured planes.

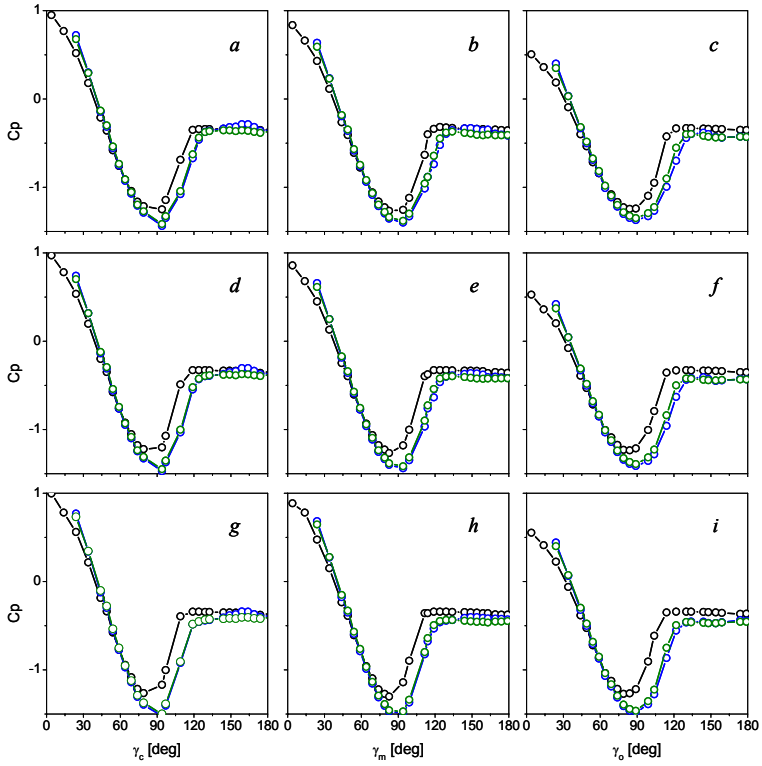

Figure 17. *Static baseline pressure profiles at the window elevation angle γ = 139° and M = 0.3 (a – c), 0.4 (d – f), and 0.5 (g – i) in the central (a, d, g), middle (b, e, h), and the outer (c, f, i) planes for the base turret geometry (—), added short (—) and long (—) forward partition plate.*

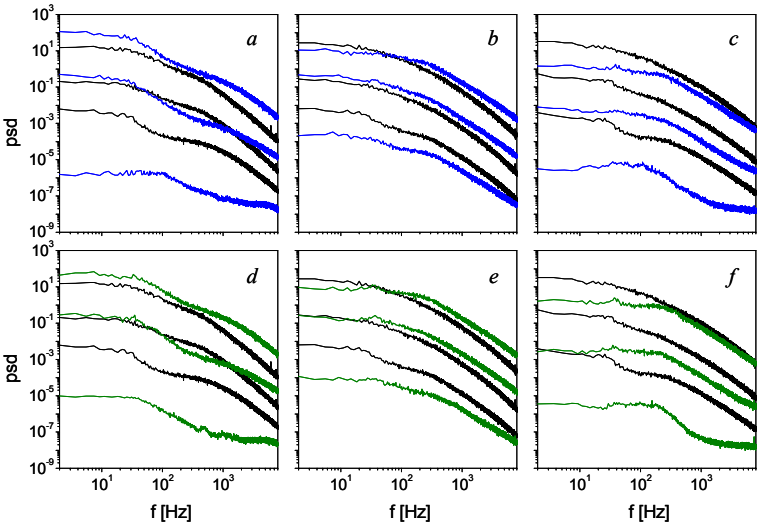

Figure 18. *Power spectra of the baseline-flow velocity fluctuations (M = 0.3) for the base turret geometry (—) and modified geometry with forward short (—) and long (—) splitter plates at γ = 145° measured by the HW1 (a,d), HW2 (b,e), and HW3 (c,f) at the high-speed edge (lowest pair), middle (middle pair) and low-speed edge (highest pair) of the shear layer. Pairs of spectra for the middle and low-speed edge are offset by two and four decades, respectively.*

The second significant feature of the altered pressure profiles implies a strong acceleration of the outer flow around the turret, as pressure levels decrease notably starting at about $\gamma_{c,m,o} = 70°$. Not only that the favorable effect does not diminish in an outward direction across the optical window, but it appears that the favorable effect becomes even more pronounced (e.g., compare Figures 17*a* and *c*). The third alteration of the baseline profiles is manifested at the very upstream end of the hemispherical cap, where the displaced stagnation point on the hemispherical surface increases the local static pressure. In addition to these three major effects, it should be emphasized that the favorable effect on the flow does not diminish with the increase in the free stream Mach number from $M = 0.3$ to 0.5. These finding suggest that the present passive modifications of the base turret geometry would induce a significant flow separation delay even beyond the range of free stream speeds under investigation, i.e., for $M > 0.5$. Additional static pressure measurements at two other elevation angles (not shown) just confirm invariance of the baseline flow over the turret with partition plates, as the baseline flows do not depend on the optical window elevation angle.

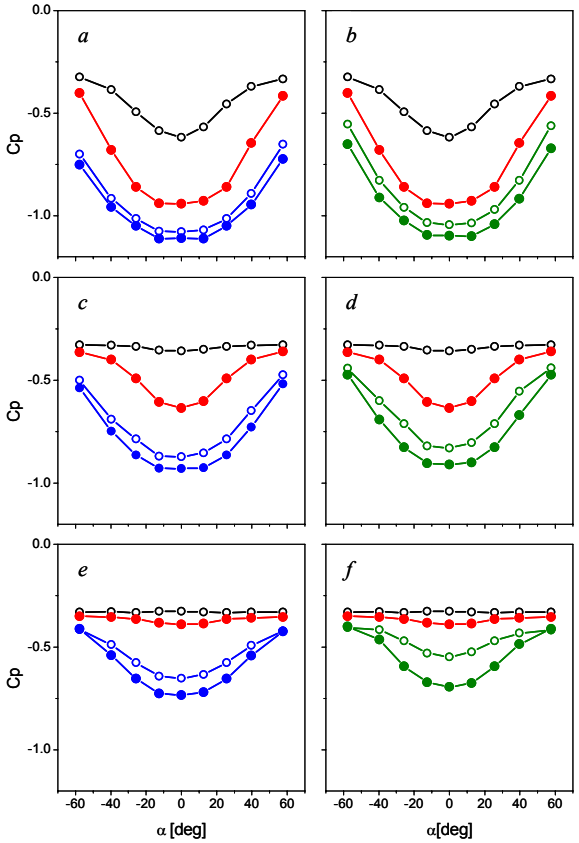

Figure 19. *Static pressure distributions about the optical window center ($\alpha = 0°$) at $M = 0.3$ and the window elevation angles $\gamma = 139°$ (a–b), 145° (c–d), and 150° (e–f) for the base turret geometry (—), added short (—) and long (—) forward partition plate. Open symbols mark the baseline flow and the corresponding solid symbols mark the full active flow control case.*

The next characterization of the passive control effect relative to the base turret geometry was done in the spectral domain using single-sensor hot-film anemometry, analogous to characterization done for active flow control, shown in Figure 13. Hot-film measurements were done at three downstream locations, HW1, HW2, and HW3, as described in Section II. As an illustration of the splitter plate effect on the separating-flow shear layer, velocity fluctuation spectra are shown in Figure 18 for the base turret geometry and added short and long partition plates at $M = 0.3$ and $\gamma = 145°$. Each plot shows three pairs of spectra, where the bottom pair corresponds to the high-speed edge of the shear layer, the middle pair corresponds to the shear layer bulk (and is offset by 10^2 in magnitude), and the upper pair corresponds to the low-speed edge of the shear layer (and is offset by 10^4 in magnitude). Resulting spectra seem virtually independent of the partition plate size, as energy distributions are both in qualitative and quantitative agreement. Therefore, it is suggested that the central wake dynamics is not sensitive to the selection of a partition plate. In either case, near-field dynamics (Figures 18*a*,*d*) shows significant broadband reduction in the fluctuating energy over the high-speed edge of the shear layer, an increase of the energy at both the small- and large-scales, with some suppression in the midrange within the shear layer bulk, and mostly broadband increase in energy along the low-speed edge of the shear layer. These characteristics reflect postponed separation and the fact that shear layer is drawn closer to the turret surface, as already surmised from pressure profiles (Figure 17) and surface oil-flow visualization (Figures 15 and 16). Further downstream (Figures 18*b*,*e*), lowered broadband suppression at the high-speed edge is accompanied by a smaller increase in energy in the bulk and along the low-speed edge, where some decrease of energy is still measured at the largest scales. Finally, at the farthest downstream measurement location (Figures 18*c*,*f*), suppression of energy over large-scale to broadband motions dominates each spectrum, regardless of the cross-stream position. Spectral results for different elevation angles are omitted, as they only show invariance in the flow dynamics with the elevation angle change.

Figure 19 demonstrates the incremental effects of passive and hybrid (simultaneous passive and active) flow control relative to the base turret geometry and pure active flow control on the mean flow upstream from the optical window. Static pressure distributions just upstream from the turret optical window are shown for $M = 0.3$ and three

elevation angles, γ = 139°, 145°, and 150°, with and without partition plates, and with and without active flow control. At the lowest elevation angle (Figures 19*a*,*b*) pure active flow control has the strongest impact among all elevation angles. Passive addition of either plate delays the separation even more, as evidenced by the additional pressure drop. Furthermore, the passive flow control effect is more evenly distributed over the optical window span. Upon activation of hybrid flow control an extra additive effect of the active flow control is seen in further favorable preconditioning of the flow upstream from the optical window. At the next elevation angle (Figures 19*c*,*d*), a similar but weaker effect is seen in both the passive and hybrid flow control. Presumably the most important effect is seen at the highest elevation angle (Figures 19*e*,*f*), where the flow over the base turret geometry is fully separated upstream from the optical window. Passive and hybrid flow control are capable of fully recovering the non-separated flow condition upstream from the optical window, which were shown to have significant ramification of suppression of the optical aberrations even at this most-backward looking angle[25]. In comparison of short and long partition plates as components in the hybrid flow control, it should be also emphasized that regardless of the plate used, hybrid flow control results are almost identical. This stems from the fact that if the effect of passive control is weaker, the active part of the hybrid control yields a stronger increment, and vice versa (see, for example, Figures 19*e* and *f*).

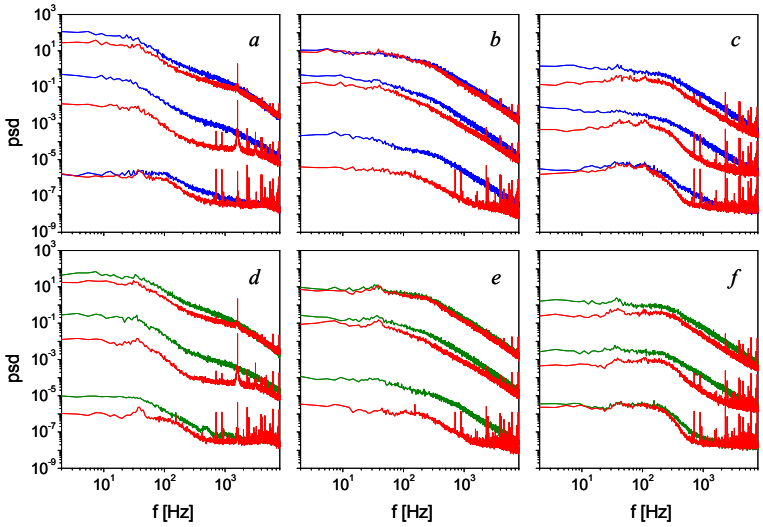

Figure 20. *Power spectra of the baseline and actuated (—) velocity fluctuations (M = 0.3) for the modified turret geometry with forward short (—) and long (—) splitter plates at γ = 145° measured by the HW1 (a,d), HW2 (b,e), and HW3 (c,f) at the high-speed edge (lowest pair), middle (middle pair) and low-speed edge (highest pair) of the shear layer. Pairs of spectra for the middle and low-speed edge are offset by two and four decades, respectively.*

Therefore, either passive modification of the base turret geometry induces larger separation delay than in the case of active flow control on the base geometry. Further outer flow acceleration measured in further reduction of the mean surface pressure is achieved when the active flow control is applied to the modified turret geometry. It should be also noted that static pressure profiles reflect only a static component of the active flow control effect on the flow that is expressed through the separation delay – active suppression of the large scale motions in the wake are assessed by supplemental diagnostics, such as the hot-film and direct optical measurements.

Similar to the characterization of the impact on the shear layer dynamics between baseline and passive flow control at γ = 145° (Figure 18), difference in spectral content of the hybrid and passive flow control is assessed from the analogous measurements shown in Figure 20. It is significant that the hybrid flow control results in an overall suppression in broadband energy of velocity fluctuations regardless of either streamwise or cross-stream measurement position. Furthermore, with some minor differences, the effect is quite similar at γ = 150° (not shown), which indicates spatial robustness of the active flow control. Much as the static pressure distributions in Figure 19, comparison of spectral properties of the shear layers in Figures 13, 18, and 20 suggests even more that there is a clear advantage of the hybrid flow control over passive and active control in overall suppression of turbulent fluctuations in the shear layer

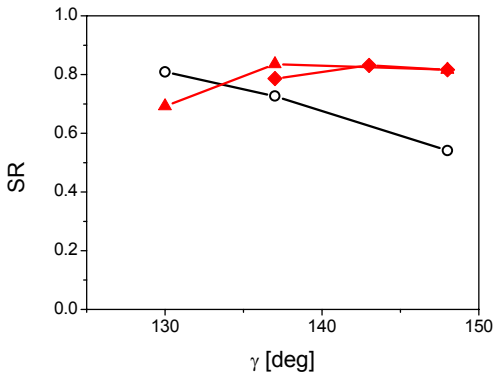

Figure 21. *Strehl ratio with the turret elevation angle for the baseline (○) and the hybrid flow control using the short (▲) and long partition plate (♦).*

separating off the turret.

Finally, an illustration of the resulting aero-optical effect of the hybrid flow control is shown in Figure 21. A detailed presentation of the accompanying aero-optical flow diagnostics is done by Gordeyev et al.[25]. Here, only the flow control effect is shown in terms of a Strehl ratio *SR*, i.e., ratio of the laser beam intensity at the detection plane to the theoretical maximum intensity of a perfect imaging system working at the diffraction limit. It is calculated using the large aperture approximation and a $\lambda = 1$ μm laser wavelength as $SR = \exp(-(2\pi \cdot OPD\text{rms}/\lambda)^2)$, where the spatial root-mean-square of the beam's optical path difference OPDrms is measured by the 2D wavefront sensor at $M = 0.3$. First, it should be noted that, similarly to the aerodynamic characterization, no significant difference is seen between the short and long partition plates as passive components in the hybrid control. Measurement at the lowest elevation angle and short passive plate indicates a decrease in *SR* relative to the baseline, and it may be attributed to the excessive active control (kept constant for all elevation angles) at this angle, for which even the baseline *SR* is very high. Next, it is interesting to note that using hybrid control, nearly invariant Strehl ratio is achieved for all higher elevation angles, at $SR \approx 0.8$. As the *SR* substantially decreases with an increase in elevation angle, it is implied that the highest *SR* "recovery" is achieved for the highest elevation angle, as the baseline *SR* is increased by about 50%.

VI. Conclusions

The effectiveness of both active and hybrid flow control on the flow over a turret is investigated experimentally at $M = 0.3 - 0.5$ and $Re_D = 4.4–7.4 \cdot 10^6$. The main motivation for this work is the objective of suppressing optical aberrations within the separated flow over a conformal optical window embedded in the hemispherical cap of a cylindrical turret model. Active flow control is effected via direct, small-scale actuation by arrays of synthetic jets distributed upstream from the optical window. In a case of hybrid flow control, a forward passive partition plate is added for a global flow alteration in tandem with active control. Single partition plate geometry is tested in two lengths: partitions that extend $R/2$ and R upstream from the turret, which are mounted at the interface between the cylinder and hemisphere. The effects of actuation on the base flow at three elevation angles of the optical window are assessed from the surface static pressure distributions, oil-flow visualization, and hot-film measurements within the separated flow.

Compared to the previous test of active flow control in a similar geometry and flow conditions[17], spatial re-distribution of the control actuators is shown to enhance the control effects outward from the central symmetry plane. Surface oil-flow visualization of the baseline flows over the modified turret geometry by additions of either partition plate showed significant reduction in the wake reattachment length for about 30% at $M = 0.3$. Induced necklace vortices at the upstream juncture between the plates and hemisphere are shown to displace the stagnation point on the hemisphere from $\gamma = 0°$ to 9° and 17° for the long and short partition plates, respectively. Static pressure measurements indicate further that both partition plates induce significant separation delay $\Delta\gamma_s \approx 20°$ across the optical window. Moreover, such a strong separation delay is persistent over the full span of the tested Mach numbers $M = 0.3 - 0.5$. Spanwise static pressure distributions upstream from the optical window indicate that passive flow control induces stronger separation delay than active flow control, while their simultaneous application in the hybrid control mode yields the best results. Furthermore, it is interesting to note that hybrid control recovers almost identical static pressure fields upstream from the optical window regardless which partition plate is utilized. Spectral characterization of the separated flow by measurements of the velocity fluctuations showed that addition of the partition plate to the base turret geometry induces a near-field effect that varies across the shear layer, but that eventually suppresses broadband fluctuation energy across the shear layer further downstream from the turret. Such a favorable effect is further enhanced by addition of active flow control in the hybrid control configuration, for which it is measured that it always further reduces broadband energy of the velocity fluctuations regardless of the downstream and cross-stream position within the shear layer. Overall, it is concluded that hybrid flow control always induces the best aerodynamic alteration of the wake in any of the aspects that the active, passive, and hybrid flow control were analyzed. Furthermore, only subtle differences are measured between the two partition plates that were tested, with both of these passive modifications resulting in substantial and similar flow separation delay and suppression of the turbulent energy within the ensuing wake.

Although accompanying aero-optical flow characterizations are presented in depth by Gordeyev et al.[25], some overall results are shown here, verifying that measured aerodynamic improvements due to the hybrid control are related to the enhancement in the aero-optical transmission through the controlled flow. Thus, it is shown that the Strehl ratio of the beam traversing the separated flow under the hybrid control becomes nearly independent of the elevation angle between $\gamma = 137° - 148°$. Knowing that the baseline Strehl ratio significantly decreases with an

increase in elevation angle, it follows that the highest improvement in the Strehl ratio of about 50% is achieved for the highest elevation angle.

Acknowledgment

This work has been supported by the Air Force Research Laboratory, Air Vehicle Directorate, W-PAFB, OH and the Boeing Company. Support by the AFRL program manager Donnie Saunders and SARL-tunnel personnel is greatly appreciated.

References

[1]Sutton, G. "Aero-optical foundations and applications", AIAA J., Vol, 23, 1985, pp 1525-1537.

[2]Gilbert, J. and Otten, L. J. (eds), *Aero-Optical Phenomena*, Progress in Astronautics and Aeronautics, Vol. 80, AIAA, New York, 1982.

[3]Tatarskii, V. I. and Zavorotnyi, V. U, "Wave propagation in random media with fluctuating turbulent parameters,", *J. Opt. Soc. Am. A*, Vol. 2, No. 12, 1985, pp. 2069-2076.

[4]Jumper, E. J., and Fitzgerald, E. J., "Recent advances in aero-optics", *Progress in Aerospace Sciences*, Vol. **37**, 2001, pp.299-339.

[5]Dimotakis, P. E., Catrakis, H. J., and Fourguette, D., C., "Flow structure and optical beam propagation in high-Reynolds-number gas-phase shear layers and jets", *J. Fluid Mech.*, Vol. 433, 2001, pp. 105-134.

[6]Fitzgerald, E. J. and Jumper E. J., "The optical distortion mechanism in a nearly incompressible free shear layer," *J. Fluid Mech.*, Vol. 512, 2004, pp. 153-189.

[7]Hunt, J. C. R., Abell, C. J., Peterka, J. A., and Woo, H., "Kinematical studies of the flows around free or surface-mounted obstacles; Applying topology to flow visualization", *J. Fluid Mech.*, Vol. 86, 1978, pp. 179-200.

[8]Leder, A., Grebin, U., Hassel, E., Kashkoul, Y., and Ackl A., "3D-Flow structures behind a circular cylinder with hemispherical head geometry", *Proc. Appl. Math. Mech*,. Vol. 3, 2003, pp 40–43.

[9]Vukasinovic, B., Brzozowski, D., and Glezer, A., "Fluidic control of separation over a hemispherical turret", AIAA J., Vol. 47, No. 9, 2009, pp. 2212-2222.

[10]Woszidlo, R., Taubert, L., and Wygnanski, I., "Manipulating the flow over spherical protuberances in a turbulent boundary layer", AIAA J., Vol. 47, No. 2, 2009, pp. 437-450.

[11]Snyder, C. H., Franke, M. E., and Masquelier, M. L., "Wind-tunnel tests of an aircraft turret model", *J. Aircraft*, Vol. 37, 2000, pp. 368-376.

[12]Gordeyev, S., Jumper, E. J., Ng, T. T., and Cain, A. B., "The optical environment of a cylindrical turret with a flat window and the impact of passive control devices", *AIAA Paper* 2005-4657, 2005.

[13]Purhoit, S. C., Shang, J. S., and Hankey, W. L., "Effect of suction on the wake structure of a three-dimensional turret", *AIAA Paper* 83-1738, 1983.

[14]Vukasinovic, B. and Glezer, A., "Control of a separating flow over a turret*", AIAA Paper* 2007-4506, 2007.

[15]Vukasinovic, B., Glezer, A., Gordeyev, S., Jumper, E., and Kibens, V., "Active control and optical diagnostics of the flow over a hemispherical turret, *AIAA Paper* 2009-598, 2008.

[16]Morgan, P. and Visbal, M., "Numerical simulations investigating control of flow over a turret", *AIAA Paper* 2009-574, 2009.

[17]Vukasinovic, B., Glezer, A, Gordeyev, S., Jumper, E., and Kibens, V., "Fluidic Control of a Turret Wake, Part I: Aerodynamic Effects", *AIAA Paper* 2009-816, 2009.

[18]Gordeyev, S., Jumper, E., Vukasinovic, B., Glezer, A., and Kibens, V., "Fluidic Control of a Turret Wake, Part II: Aero-Optical Effects", *AIAA Paper* 2009-817, 2009.

[19]Wallace, R., Andino, M., Glauser, M., Camphouse, C., Schmit, R., and Myatt, J., "Flow characteristics of active control around a 3D turret", *AIAA Paper* 2009-573, 2009.

[20]Gordeyev, S. and Jumper, E., "Fluid dynamics and aero-optical environment around turrets", *AIAA Paper* 2009-4224, 2009.

[21]Vukasinovic, B., Glezer, A., and Rusak, Z., "Experimental and numerical investigation of controlled, small-scale motions in a turbulent shear layer*", Proc. 3rd International Symposium of Integrating CFD and Experiments in Aerodynamics*, June 2007, U.S. AFA, CO, USA.

[22]Zubair, F.R., Freeman A.P., Piatrovich S., Shockro J., Ibrahim Y.N., and Catrakis, H.J., "Large scale turbulence suppression control for direct reduction of aero-optical aberrations", AIAA Paper 2007-4008, 2007.

[23]Oljaca, M. and Glezer, A., "The effects of induced dissipative small-scale motions and mixing on optical distortion in a plane shear layer", *J. Fluid Mech.*, Vol. 619, 2009, pp. 295-329.

[24]Schonberger, J. R., Fuhs, A. E., and Mandigo, A. M., "Flow control for an airborne laser turret", J. Aircraft, Vol. 19, No. 7, 1982, pp. 531-537.

[25]Gordeyev, S., Jumper, E., Vukasinovic, B., Glezer, A., and Kibens, V., "Hybrid Control of a Turret Wake, Part II: Aero-Optical Effects", *AIAA Paper* 2010-438, 2010.

[26]Achenbach, E., "Experiments on the flow past spheres at very high Reynolds numbers", *J. Fluid Mech.*, Vol. 54, No. 3, 1972, pp. 565-575.